The International Journal of Advanced Manufacturing Technology (2021) 116:3663–3676
https://doi.org/10.1007/s00170-021-07612-3

ORIGINAL ARTICLE

Experimental studies on material removal mechanisms in ultrasonic assisted grinding of SiC ceramics with a defined grain distribution brazed grinding wheel

Kai Ding[1] · Qilin Li[1] · Changdong Zhang[2]

Received: 25 November 2020 / Accepted: 29 June 2021 / Published online: 21 July 2021

Abstract
Ultrasonic assisted grinding (UAG) is one of the most suitable methods for the processing of hard and brittle materials such as silicon carbide (SiC). During UAG of SiC, the machining quality is directly determined by the material removal mechanism. However, the research on the material removal mechanism for UAG of SiC is still not sufficiently developed. To achieve better comprehension of the material removal mechanism in UAG of SiC, this study conducted both UAG and conventional grinding (CG) tests with a brazed grinding wheel with defined grain distribution. The material removal mechanism in UAG of SiC was studied by comparing the ground surface/subsurface micro-morphology, surface roughness, grinding force, and specific grinding energy between both processes. The results showed that the material removal mechanism experienced a transition from ductile removal to brittle fracture with increasing undeformed chip thickness in both UAG and CG. In addition, the ground surface roughness, grinding force, and subsurface breakage size increased with increasing undeformed chip thickness, while the specific grinding energy first decreased rapidly and then stabilised. Compared with conventional grinding, UAG always resulted in lower surface/subsurface breakage, surface roughness grinding force, and specific grinding energy under identical operating conditions.

Keywords Material removal mechanism · Ultrasonic assisted grinding · Defined grain distribution brazed grinding wheel · Ground surface/subsurface micro-morphology · Specific grinding energy

1 Introduction

Silicon carbide (SiC) ceramics possesses superior properties such as high specific stiffness, good thermal stability, low thermal deformation coefficient, and low density. Because of these advantages, today, SiC is widely used to prepare space reflection mirrors. Generally, because of the high hardness and brittleness of this material, conventional grinding (CG, without ultrasonic) or ultrasonic assisted grinding (UAG) with a diamond wheel has always been considered as the most suitable process [1, 2].

UAG is a hybrid process that combines diamond grinding with ultrasonic machining [3–5]. Over the last few decades, many studies have confirmed that UAG offers many advantages for the processing of hard and brittle materials such as low grinding force, high machining quality, and low surface/subsurface breakage. Uhlmann [6] used UAG on Si_3N_4 and ZrO_2 ceramics and found that UAG caused a reduction in thermal loads and process forces. Gao et al. [7] concluded that in comparison to CG, UAG of nano-zirconia could more easily implement ductile-regime grinding and acquire higher quality ground surface. Wang et al. [8] conducted grinding tests of Si_3N_4, the results of which indicated that UAG significantly reduced the grinding force and ground surface roughness. Zheng et al. [9] demonstrated that UAG caused lower grinding force and higher material removal rate compared with CG. Thus, UAG is most suitable for the machining of hard and brittle materials such as advanced ceramics. Guo et al. [1] demonstrated that there were no cracks on the ground micro-structured surfaces produced by ultrasonic assisted grinding, and the ductile material remove behaviour dominated the grinding process.

✉ Kai Ding
dingkai@jsut.edu.cn

[1] School of Mechanical Engineering, Jiangsu University of Technology, Changzhou 213001, China

[2] School of Mechanical Engineering, Nanjing University of Science and Technology, Nanjing 210094, China

When used for optical components (such as reflection mirrors), these require a high-quality processed surface. In general, the machined surface quality of advanced ceramics is directly affected by the material removal mechanisms during the grinding process [10, 11]. In 1991, Bifano [12] proposed a ductile-regime grinding method for the processing of brittle materials and concluded that if the dimensional scale of material removal was sufficiently small, material removal would proceed by a mechanism of plastic flow rather than fracture. To this day, the generally accepted criteria for the ductile-regime grinding of hard and brittle materials are that the maximum undeformed chip thickness is smaller than the critical depth of the cut. It can be concluded that this criterion is also true for UAG, and it forms the base for carrying out analysis of material removal modes for hard brittle materials. A number of research findings about material removal mechanisms during UAG have been reported before. In 1995, Pei et al. [13] demonstrated that under specific conditions, plastic flow dominated the material removal process during rotary ultrasonic machining of hot-pressed silicon nitride and proposed a material removal rate model based on the ductile mode [14]. Liang et al. [15] conducted elliptical UAG of monocrystal sapphire using a single diamond abrasive grain. Their studies showed that the critical depth of the resulting cut was significantly increased via ultrasonic assistance, i.e. elliptical UAG was highly effective for ductile-mode machining of monocrystal sapphire. Jain [16] reported that the percentage of ductile mode as well as the surface finish achieved in rotary ultrasonic machining was higher compared with that of the grinding process. Chen et al. [17] and Zhou et al. [18] also reported similar results in their studies of simulation analysis and single grit scratching method, respectively. Li et al. [19] conducted grinding experiments with or without vibration assistance and concluded that vibration facilitated the ductile removal of brittle material because it decreases the undeformed chip thickness and changes of stress condition within the undeformed chip zone. Zhao et al. [20] designed an ultrasonic assisted elliptical vibration system and conducted grinding experiments of nano-ZrO_2. The results showed that UAG could expand the plastic processing domain, as well as improve the surface and fatigue strength of nano-ZrO_2 (to some extent). In summary, intensive research on material removal mechanisms during UAG of hard brittle materials has been conducted. However, the effect of ultrasonic vibration on the material removal mechanisms during grinding process still remains insufficient and requires further work.

In general, the maximum undeformed chip thickness is a comprehensive coefficient that is determined by both grinding parameters and the surface status of the grinding wheel and exerts an important influence on the grinding forces and grinding energy [21–23]. Therefore, it is very important to obtain quantitative descriptions of the maximum undeformed chip thickness both for CG and UAG. However, for a traditional grains disorderly arranged grinding wheel, because of the stochastic nature of grains, break out, or quick wear at wheel working layers, the maximum undeformed chip thicknesses are distributed over an interval rather than being single valued [23]. Under this condition, many researchers are beginning to develop defined grain distribution grinding wheels to achieve uniform maximum undeformed chip thickness during the grinding process. Currently, the main preparation methods for defined grain distribution grinding wheels are electroplating and brazing processes [24–27]. Compared with electroplated grinding wheels, brazed grinding wheels possess high grit protrusion, strong grit bond adhesion, and long service life [28–30]. Accordingly, the brazed grinding wheel has become one of the most suitable tools for the grinding of hard and brittle materials. To this day, many researchers have reported applications of brazed diamond wheels in the CG of hard brittle materials such as oxide ceramic [31], SiC [28], silicon nitride [32], alumina, and zirconia [33]. However, related studies during UAG have not been reported to date.

However, building the maximum undeformed chip thickness model forms the base for conducting quantitative analyses of material removal mechanisms during the grinding process. For the CG method, Hecker et al. [34] proposed an undeformed chip thickness model that considers kinematic conditions, material properties, wheel micro-structure, and dynamic effects. Malkin [35] built an undeformed chip thickness model based on the analysis of the geometrical relationship between the grain and the workpiece. Agarwal et al. [36, 37] developed a new analytical undeformed chip thickness model for ceramics via calculating the average volume of grinding layer based on the stochastic nature (i.e., the random geometry and the random distribution of cutting edges) of the grinding process. For UAG, Jain et al. [16] and Bertsche et al. [38] presented undeformed chip thickness models under the approximation condition, i.e. using a triangular wave rather than a sinusoidal wave. Obviously, this study can draw on the experience of the above studies.

In this paper, with the objective to study the material removal mechanisms for UAG of SiC, grinding tests were conducted with a defined grain distribution brazed diamond grinding wheel both with and without ultrasonic vibration, i.e. with the methods of UAG and CG, respectively. The ground surface micro-morphology produced under different grinding parameters, i.e. different maximum undeformed chip thicknesses for both processes were observed. Additionally, subsurface breakage, ground surface roughness, grinding force, and specific grinding energy were also compared between both processes. Based on this approach, the effect of ultrasonic vibration on the material removal mechanism (based on the defined grain distribution brazed diamond grinding wheel) was studied.

2 Assessing the method of the material removal mechanism during UAG

2.1 Kinematic analysis and undeformed chip thickness

The UAG process is illustrated in Fig. 1. In this study, the ultrasonic vibration is applied parallel to the ground surface. During UAG, a cup diamond wheel rotates at a certain speed and vibrates along the Z-direction at a frequency of 20–30.4 kHz while simultaneously continuing to move toward the Y-direction. The trajectory of a single diamond grain can be described by the set of Eq. (1):

$$\begin{cases} X(t) = R\sin(\omega t) + v_w t \\ Y(t) = R\cos(\omega t) \\ Z(t) = A\sin(2\pi f t) \end{cases} \quad (1)$$

where R represents the radius of the tool, A represents the amplitude of vibration, ω represents the angular velocity, v_w represents the feed rate, f represents the vibration frequency, and t represents the time.

Based on Eq. (1), the trajectory of a single grain during UAG is shown in Fig. 2. It follows a three-dimensional (3D) sinusoidal curve and grain trajectories in the grinding zone overlap accordingly.

The maximum undeformed chip thickness a_{Cgmax} during CG is illustrated in Fig. 3(a). This figure shows that the relative motion of the cutting grain, with respect to the ground surface, generates a removed chip with a curved longitudinal shape in CG [37]. Regarding the ideal grains spacing on the grinding wheel working surface during CG, Malkin [35] proposed a widely accepted maximum undeformed chip thickness model a_{Cgmax} as:

$$a_{Cgmax} = 2\Delta x\left(\frac{v_w}{v_s}\right)\left(\frac{a_p}{d_s}\right)^{1/2} \quad (2)$$

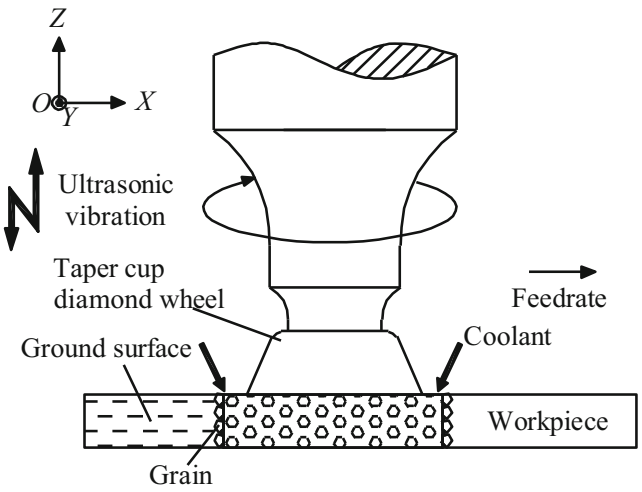

Fig. 1 Ultrasonic assisted grinding

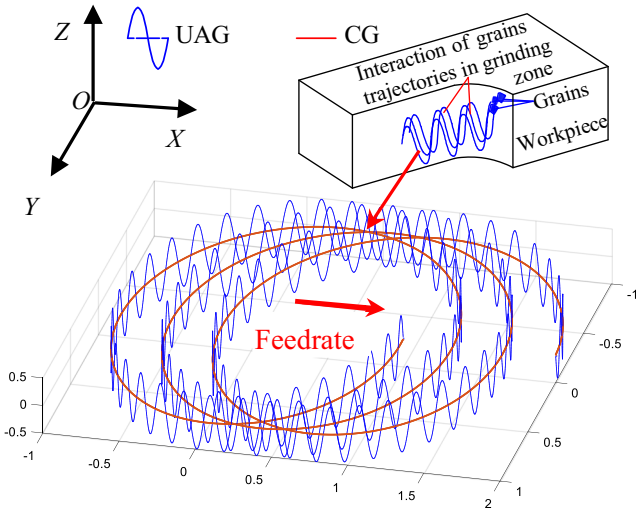

Fig. 2 Overlapping of grains trajectories

where Δx represents the ideal grains circumferential interval, v_s represents the grinding speed, a_p represents the grinding depth, and d_s represents the diameter of the grinding wheel.

However, compared with CG, the ultrasonic vibration is superimposed on the z direction during UAG, and the maximum undeformed chip thickness a_{Ugmax} is consequently formatted as illustrated in Fig. 3(b). As can be seen in Figures 2 and 3(b), a complex 3D geometric relationship exists between the grain and the ground surface. Bertsche et al. [38] and Jain et al. [16] proposed the models of a_{Ugmax} in rotary ultrasonic machining (RUM) independently as Eqs. (3) and (4):

$$a_{Ugmax} = \left(\frac{v_w}{v_s}\right)^{\frac{2}{3}}\left(\frac{4}{27}\frac{\rho\pi d_g^3}{C}\right)^{\frac{1}{3}} \quad (3)$$

where v_w represents the feed rate, v_s represents the grinding speed, ρ represents the density of the abrasive grains, d_g represents the diamond grain diameter, and C represents the diamond tool concentration.

$$a_{Ugmax} = \sqrt{\frac{v_w\lambda^2}{v_s C_{dus} 4 r_{us} e^2}}\sqrt{\frac{d_a}{D_o}} \quad (4)$$

where λ represents the ultrasonic wavelength, C_{dus} represents the number of cutting edges per unit area in dynamic condition in RUM, r_{us} represents the ratio of mean chip width to mean un-deformed chip thickness in RUM, e represents the distance travelled by an abrasive grain in quarter ultrasonic wavelength, d_a represents the axial depth of cut, and D_o represents the outer diameter of the wheel.

Based on their own mathematical models, Bertsche et al. [38] concluded that the amplitude and frequency in RUM had no effect on the a_{Ugmax}, i.e. a_{Ugmax} was identical with a_{Cgmax}, while Jain et al. [16] concluded that a_{Ugmax} was lower than a_{Cgmax}. In summary, there is no widely applicable theoretical

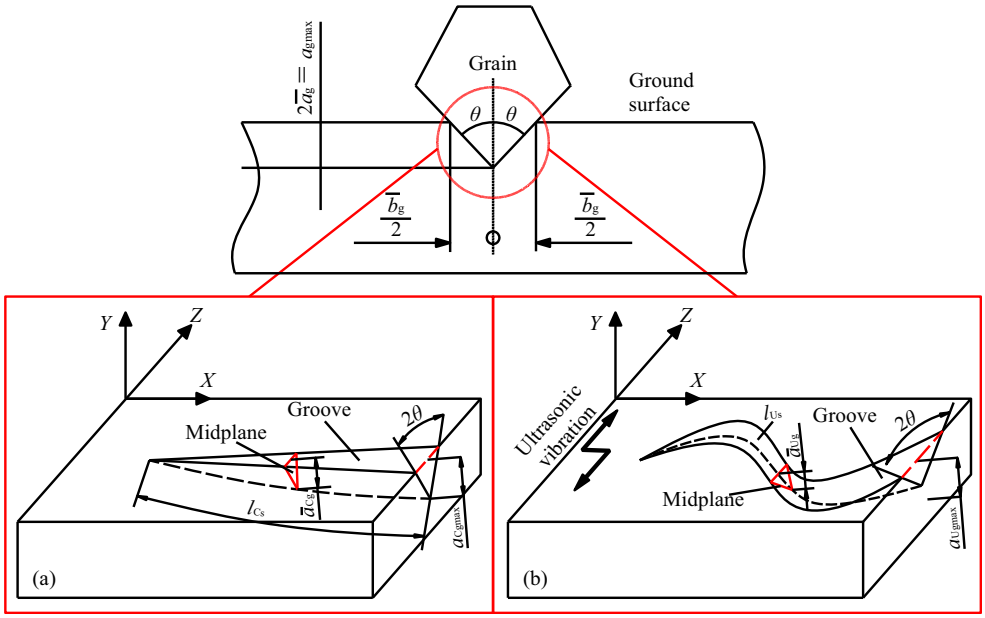

Fig. 3 Schematic diagram of single grain grinding and (a) a_{Cgmax} in conventional grinding (CG) as well as (b) a_{Ugmax} in ultrasonic assisted grinding (UAG)

model for a_{Ugmax} in UAG until now. However, what the two models have in common is that for a certain amplitude and frequency in RUM, a_{Ugmax} also increases with increasing feed rate v_w while decreases with increasing grinding speed v_s. In addition, Eq. (4) also illustrates that a_{Ugmax} increases with increasing axial depth of cut d_a. Thus, with the objective to study the transition of material removal mechanisms with changing a_{Ugmax} in UAG of SiC, experimental parameters are set to produce different a_{Ugmax} based on Eqs. (3) and (4). In addition, corresponding a_{Cgmax} calculated by Eq. (2) in CG are supplied as reference values.

2.2 The critical depth of the cut

As stated in the introduction, regarding the CG of hard brittle materials, the material removal mechanism will change from fracture to plastic flow when the a_{Cgmax} reduces to a certain value (i.e. the critical depth of the cut). Based on the Griffith fracture propagation criterion and microindentation techniques, Bifano [12] proposed a critical depth of the cut model, which can be expressed as:

$$h_c = 0.15\left(\frac{E}{H}\right)\left(\frac{K_{Ic}}{H}\right)^2 \tag{5}$$

where E represents the elastic modulus, H represents the hardness, and K_{Ic} represents the static fracture toughness.

Eq. (5) was acquired by microindentation techniques under slow loading, similar to static conditions. However, during the actual grinding process, grinding forces emerge that are caused by elastic-plastic deformation and friction between the workpiece and grinding wheel. Therefore, to accurately study the material removal mechanism, a number of scholars [39, 40] revised the critical depth of the cut model under conditions closer to the grinding process. Their results showed that the dynamic fracture toughness K_{Id} is about 30% of K_{Ic}. Accordingly, Eq. (6) can be revised as:

$$h_c = 0.15\left(\frac{E}{H}\right)\left(\frac{K_{Id}}{H}\right)^2 = 0.15\left(\frac{E}{H}\right)\left(\frac{0.30K_{Ic}}{H}\right)^2 \tag{6}$$

Based on Eqs. (2) and (6), the quantitative judging criteria of the material removal mechanism during CG of hard brittle materials is determined, i.e. brittle fracture will be the dominant material removal mechanism when $a_{Cgmax} > h_c$. Otherwise, plastic flow (i.e. ductile-regime grinding) will be the dominant mechanism when $a_{Cgmax} < h_c$. However, the effect of ultrasonic vibration on h_c is still uncertain. Consequently, it is difficult to directly build the quantitative judging criteria of the material removal mechanism during UAG of SiC. Thus, assessing the method of the material removal mechanism during UAG in this study is to conduct comparative analysis on experimental results between CG and UAG under the same experimental conditions. More specifically, experimental results for CG are mainly used as reference objects to help discuss the material removal mechanism during UAG of SiC.

3 Experimental setup and conditions

3.1 Experimental setup

UAG and CG tests were conducted at the DMG Ultrasonic 20 Linear high-speed machining centre. Fig. 4 shows the photograph of the experimental setup. In this study, the workpiece

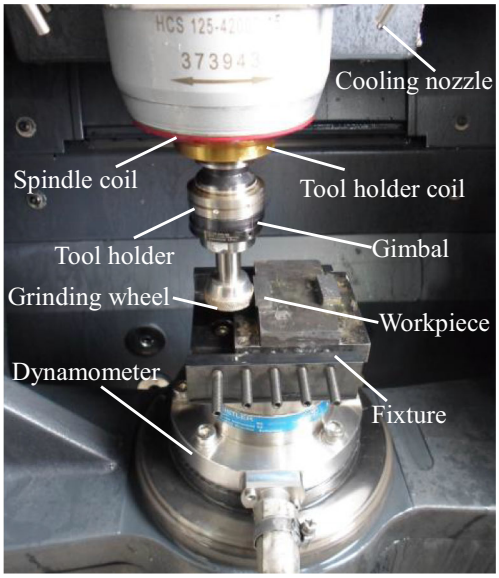

Fig. 4 Experimental setup

was spliced on a fixture with paraffin. The fixture was secured to a dynamometer via bolts. Both UAG and CG tests were conducted with an ultrasonic tool holder. The maximum rotational speed of this ultrasonic tool holder was 40000 r/min. During UAG, the ultrasonic generator converts the industrial electric signal into a high frequency electric signal (about 20–30.4 kHz). Then, this high frequency signal is transferred to a primary coil located at the end of the spindle and the secondary coil which is connected to the piezoelectric ceramic transducer. The piezoelectric ceramic transducer converts electric energy into mechanical energy, which, to conduct UAG test, is then amplified and transferred to the end face of the tool by the amplitude transformer horn. The CG test is conducted by shutting down the ultrasonic vibration system.

3.2 Experimental conditions

The workpiece material was non-pressurised sintering SiC. The micro-morphology of its polished surface is shown in Fig. 5. A number of primary randomly distributed porosities

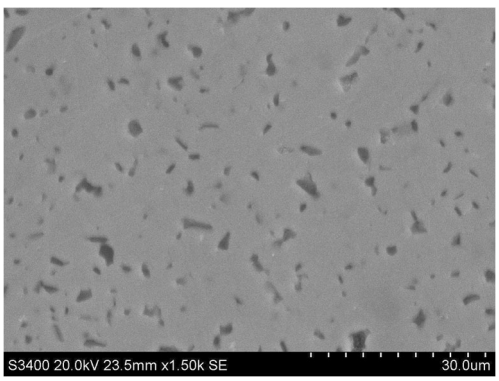

Fig. 5 Micro-morphology of SiC ceramic

with an apparent porosity of about 0.5% can be found. The mechanical properties of the workpiece are shown in Table 1. Substituting these parameters into Eq. (6), h_c of SiC for CG can be calculated as 0.0026 μm. The dimensions of the workpiece for observing the ground surface were 25 mm × 10 mm × 6 mm and for observing the subsurface, these were 25 mm × 10 mm × 3 mm.

With the objective to acquire an accurate a_{Cgmax}, a defined diamond grain distribution brazed grinding wheel, with nearly uniform grain circumferential interval Δx, was used for both UAG and CG tests, as illustrated in Fig. 6. The outer diameter, wall thickness, and abrasive layer width of the wheel were 30 mm, 3 mm, and 6 mm, respectively. The average grain size was about 150–160 μm. The grain circumferential interval was 1.25 mm, and the grain arrangement angle α was 45°. Before UAG and CG tests were conducted, the original working surface topography of the grinding wheel was observed, as shown in Fig. 7a. Abrasive grains were wrapped by a large volume of brazed filler metal. To remove these brazed filler metals and improve machining quality, a mechanical chemical method [23] was adopted to dress the brazed grinding wheel. The dressing process is shown in Fig. 8. In detail, the dressing tool contained an abrasive stone (SiC) and a Q235 steel workpiece. During the dressing process, the grinding wheel feed along the Z direction, thus cutting the abrasive stone and the Q235 steel workpiece in sequence. Fig. 7 b shows the grinding wheel topography when the volume of the removal material from the Q235 steel workpiece reached 600 mm^3. The excrescent filler alloy around the abrasive grains was effectively removed. In addition, this dressing process could improve the exposure height uniformity of grains [23]. The dressing parameters were grinding speed v_s = 9.4 m/s, feed rate v_w = 100 mm/min, and grinding depth a_p = 10 μm. For both the dressing process and grinding tests, Castrol emulsion was used as coolant through an external cooling nozzle as shown in Fig. 4. Its concentration was about 4%, and its pressure was 0.4 MPa. Table 2 summarises the settings of the machining parameters. Accordingly, a_{Cgmax} of each group of machining parameter is calculated via Eq. (2) and listed in Table 2. In addition, although no specific values available for a_{Ugmax}, it can be inferred that a_{Ugmax} increases gradually with increasing group number from Eqs. (3) to (4), just as a_{Cgmax}.

Table 1 Mechanical properties of SiC

Parameters	Value
Static fracture toughness K_{Ic}/(MPa·$m^{1/2}$)	3.2
Microhardness HV/(GPa)	28
Elastic modulus E/(MPa)	4.1×10^5

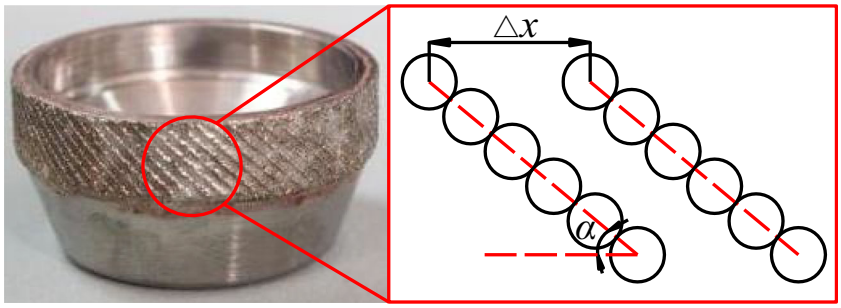

Fig. 6 Defined diamond grain distribution brazed grinding wheel

3.3 Measurement and analysis

The vibration frequency and amplitude of the tool end face were measured by a Polytec single-point vibrometer (OFV 5000). The sampling frequency was set to 300 kHz. In this study, the measured vibration frequency and amplitude of the prepared brazed grinding wheels were $f = 21.5$ kHz and $A = 3.85$ μm, respectively. The balance of the ultrasonic tool holder was measured by a Benstong dynamic banlance instrument. The grinding force was measured by a Kistler four-component piezoelectric quartz crystal dynamometer (9272) and a charge amplifier (5070A). The testing system is shown in both Fig. 4. A data acquisition card (PC-CARD D24/CTR3) was used to collect grinding force data and perform A/D conversion and was installed on the computer. DynoWare 2825D1-2 was adopted as grinding force measurement software to set measuring parameters and process the data obtained from the dynamometer. The grinding wheel topography was observed by a Hirox KH-7700 3D Video Microscope.

Subsurface breakage tests were conducted through section microscopic method as shown in Fig. 9. Before tests, all surfaces to be observed were lapped and polished to a mirror finish. Then, the two polished surfaces were glued together with paraffin. After tests, the workpieces were cleaned, and the ground surface/subsurface were gold sputtered. Then, the micro-morphology of the ground surface/subsurface produced during UAG and CG was observed by a Hitachi S-3400N II scanning electron microscope. For ease of analysis and description, the maximum depth (b) between the ground surface and the subsurface breakage area, as shown in Fig. 10, was adopted to evaluate the degree of ground subsurface breakage. In addition, in UAG, b caused was marked as b_U and as b_C in CG.

The ground surface roughness was measured with a Mahr M1 measuring instrument. The sampling length was 5.6 mm, and the measuring direction was vertical to the feed direction. The presented values represent the average of six repeated measurements.

4 Experimental results and discussion

4.1 Micro-morphology of the ground surface

Fig. 11 presents the ground surface micro-morphology of SiC, obtained in both UAG and CG under four groups of typical grinding parameters. In the order from Fig. 11 (1) to (4), the corresponding values of a_{Cgmax} and a_{Ugmax} gradually increase. As shown in Fig. 11, independent of whether UAG or CG are used, different maximum undeformed chip thicknesses caused different ground surface micro-characteristics, i.e. different material removal mechanisms. Fig. 11 (1) (a) shows the ground surface micro-morphology, obtained in CG for $v_s = 30$ m/s, $v_w = 0.05$ m/min, and $a_p = 5$ μm. Under this condition, the value of a_{Cgmax} is 0.0009 μm, which is smaller than $h_c = 0.0026$ μm. Accordingly, the ground surface is dominated by smooth areas produced by plastic removal mechanism and supplemented with porosities of different sizes. These

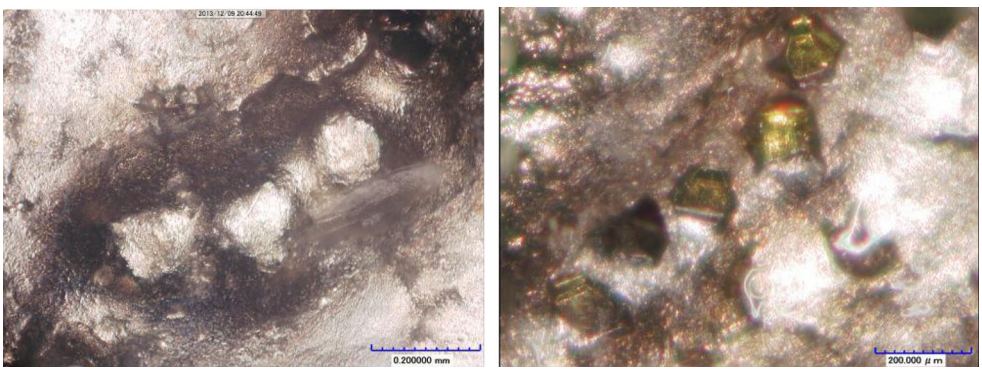

(a) Original topography (b) Dressed topography

Fig. 7 Topography of the brazed grinding wheel. **a** Original topography and **b** dressed topography

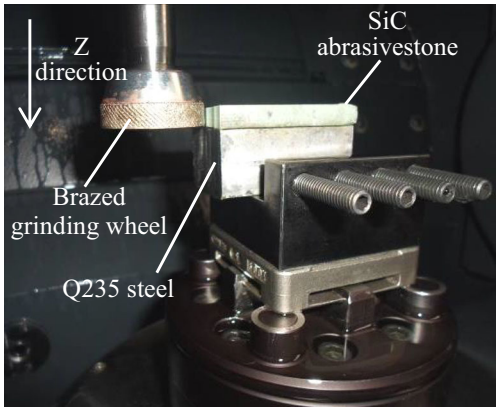

Fig. 8 Dressing setup of the brazed grinding wheel

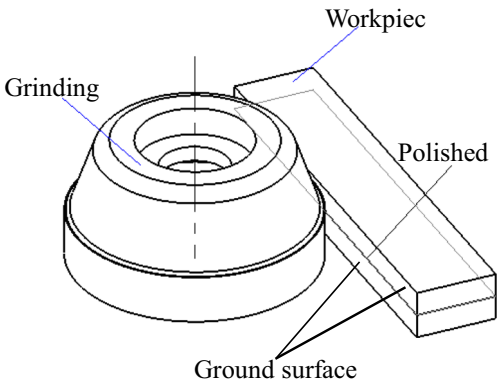

Fig. 9 Illustration of the section microscopic method

porosities mainly consist of two types, primary porosities in the workpiece as shown in Fig. 5 and porosities caused by brittle fracture during grinding. As grinding parameters changed and a_{Cgmax} increased to 0.00232 μm, which is very close to 0.0026 μm, although smooth areas and plastic grooves still remain the main micro-characteristics on the ground surface as shown in Fig. 11 (2) (a), the brittle fracture removal ratio increased apparently compared with that shown in Fig. 11 (1) (a). When a_{Cgmax} increased to 0.0268 μm, as seen in Fig. 11 (3) (a), brittle fracture becomes the main material removal mechanism and nearly no smooth areas remain. Finally, as a_{Cgmax} increased to 0.0928 μm, which far exceeds the critical depth of 0.0026 μm, as shown in Fig. 11 (4) (a), the surface breakage (including brittle fracture areas and micro cracks caused by CG) deteriorate dramatically, and the plastic removal surface completely disappeared. Instead, the ground surface shows many crushing characteristics such as micro-cracks, which resulted from the brittle fracture removal mechanisms of the material. In addition, SiC grain shedding happens locally, and micro-cracks form because of grinding stress.

The effect of ultrasonic vibration on the ground surface micro-morphology during the grinding of SiC ceramics can be analysed via comparison of the ground surface micro-morphology obtained in CG and UAG. The ground surface characteristics for CG and UAG differ with changing machining parameters, i.e. a_{Cgmax} and a_{Ugmax}. For example, for v_s = 30 m/s, v_w = 0.05 m/min, and a_p = 5 μm, the ground surface characteristics obtained in UAG are also smooth areas, produced by plastic removal mechanism and brittle fracture areas as shown in Fig. 11 (1) (b), which is identical with that obtained in CG. Compared with the ground surface obtained in CG, as presented in Fig. 11 (1) (a), nearly no difference can be seen between them. As the a_{Cgmax} and a_{Ugmax} increase further, these differences become obvious, i.e. UAG produces less brittle fracture areas than CG. As illustrated in Fig. 11 (2), for v_s = 20 m/s, v_w = 0.05 m/min, a_p = 15 μm, UAG produces more smooth area and plastic grooves compared with CG in this case. Fig. 11 (3) shows the same comparative features between CG and UAG as Fig. 11 (2). For v_s = 10 m/s, v_w = 1 m/min, and a_p = 15 μm, the surface breakage (including

Table 2 Machining parameters of UAG and CG tests

No.	Grinding speed v_s (m/s)	Feed rate v_w (m/min)	Grinding depths a_p (μm)	a_{Cgmax} (μm)	a_{Ugmax}
1	30	0.05	5	0.0009	
2	30	0.05	10	0.0013	
3	30	0.05	15	0.00154	
4	20	0.05	10	0.0019	
5	20	0.05	15	0.00232	
6	10	0.05	10	0.00378	
7	10	0.05	15	0.00464	
8	10	0.5	5	0.0268	
9	10	0.5	10	0.0378	
10	10	0.5	15	0.0446	
11	10	1	5	0.0536	
12	10	1	10	0.0756	
13	10	1	15	0.0928	

Gradually increasing

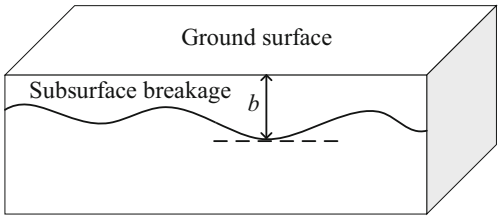

Fig. 10 Subsurface breakage size (b)

brittle fracture areas and micro-cracks) caused by UAG also deteriorate significantly. However, it is still seen that UAG produces less breakage than CG. In general, comparison of the ground surface micro-morphology obtained in UAG and CG presented in Fig. 11 illustrates that ultrasonic vibration is beneficial for the reduction of machining breakage such as brittle fracture and micro-cracks, especially for ground surfaces that contain more brittle fracture removal mechanism as shown in Fig. 11 (2), (3), and (4).

4.2 Ground surface roughness

To study the effects of a_{Cgmax} and a_{Ugmax} on the roughness of the ground surface, 13 groups of grinding parameters (as listed in Table 2) were set to conduct UAG and CG tests. The experimental results are shown in Fig. 12. Under the conditions used in this study, the scales of a_{Cgmax} is 0.0009–0.0928 μm. In addition, a_{Cgmax} and a_{Ugmax} both increases with increasing test number shown in Table 2. Because of the different values, test number was set on the bottom X-axis, and a_{Cgmax} was set on the top X-axis. Fig. 12 shows that the ground surface roughness (both in CG and UAG) increases with increasing a_{Cgmax} and a_{Ugmax}. In addition, the ground surface roughness obtained in UAG was always smaller than that obtained in CG. The coefficient K_R was defined to express the reduction percentage in the ground surface roughness for UAG compared with CG under the same conditions. As shown in Fig. 12, the K_R first increased slowly (about from 8.3 to 22.8%) with increasing a_{Cgmax} and a_{Ugmax} and then stabilised (about 18.4–22%). This phenomenon coincides with the characteristics shown in Fig. 11. Under experimental conditions, the surface roughness values obtained by UAG and CG were Ra 0.21–0.96 μm and Ra 0.23–1.23 μm, respectively.

4.3 Grinding force and specific grinding energy

Figs. 13 and 14 present the effects of a_{Ugmax} and a_{Cgmax} on both the normal grinding force and tangential grinding force. The presentation these two figures use is the same as that adopted in Fig. 12. As shown in Figs. 13 and 14, both normal grinding force and tangential grinding force increased with increasing a_{Cgmax} and a_{Ugmax}. In addition, the grinding forces produced by UAG were always lower than those produced by CG. The coefficient K_F was defined to express the reduction percentage in the grinding force for UAG compared with CG under identical conditions. The change trend of K_F with increasing a_{Cgmax} and a_{Ugmax} has the similar law as K_R, as shown in Figs. 13 and 14. With increasing a_{Cgmax} and a_{Ugmax}, the K_F of F_n first increased from 9.2 to 17.8%, and the K_F of F_t first increased from 8.1 to 16.7%. Then K_F of F_n and F_t stabilised at 15–19% and 12.7–16%, respectively.

The specific grinding energy is the energy consumed for the removal of volume material (per unit) during grinding. This is an important parameter to assess grinding mechanism and can be obtained by Eq. (7):

$$E = \frac{F_t v_s}{v_w a_p b} \tag{7}$$

Based on the measured tangential grinding force and corresponding grinding parameters, the specific grinding energy can be directly calculated according to Eq. (7). Fig. 15 shows the effects of a_{Cgmax} and a_{Ugmax} on the specific grinding energy. Clearly, the specific grinding energy decreased rapidly both in CG and UAG with increasing a_{Cgmax} and a_{Ugmax}. This phenomenon is named the "size effect" in grinding theory [30]. Concretely, when a_{Cgmax} and a_{Ugmax} are low, more plastic deformation, resulting from the ductile removal mechanism, happens, which consumes more energy. Consequently, the specific grinding energy is higher. However, with increasing a_{Cgmax} or a_{Ugmax}, brittle fracture gradually becomes the dominant material removal mechanism, and this mode requires less energy. Accordingly, the specific grinding energy decreases. In addition, as shown in Fig. 15, the specific grinding energy for CG stabilised when a_{Cgmax} increased to about 0.0037–0.0045 μm, which slightly exceeds h_c = 0.0026 μm. This indicates that the brittle fracture removal ratio enlarges apparently when a_{Cgmax} is near h_c. Similarly, the specific grinding energy for UAG also shows this regularity. These results mainly match the ground surface micro-morphology as shown in Fig. 11. However, since the tangential grinding force obtained in UAG is always smaller than that obtained in CG, the specific grinding energy consumed by UAG is always smaller than that consumed by CG.

4.4 Micro-morphology of the ground subsurface

Fig. 16 presents the subsurface micro-morphology produced by CG and UAG under different grinding parameters (i.e. different a_{Cgmax} and a_{Ugmax}). For v_s = 30 m/s, v_w = 0.05 m/min, and a_p = 5 μm, Fig. 16 (1) shows a comparison of

Fig. 11 Topographies of the ground surface obtained in UAG and CG. (I) Smooth area, (II) porosity, (III) plastic groove, (IV) brittle fracture, and (V) micro-crack. (**1**) v_s = 30 m/s, v_w = 0.05 m/min, a_p = 5 μm. (**2**) v_s = 20 m/s, v_w = 0.05 m/min, a_p = 15 μm. (**3**) v_s = 10 m/s, v_w = 0.5 m/min, a_p = 5 μm. (**4**) v_s = 10 m/s, v_w = 1 m/min, a_p = 15 μm

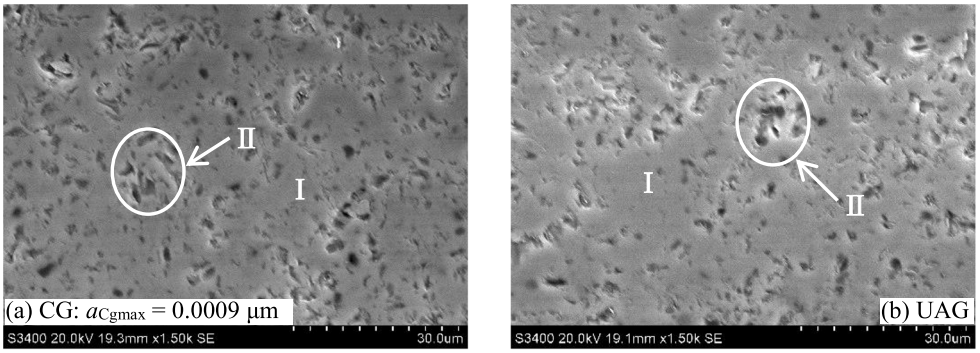

(1) v_s = 30 m/s, v_w = 0.05 m/min, a_p = 5 μm

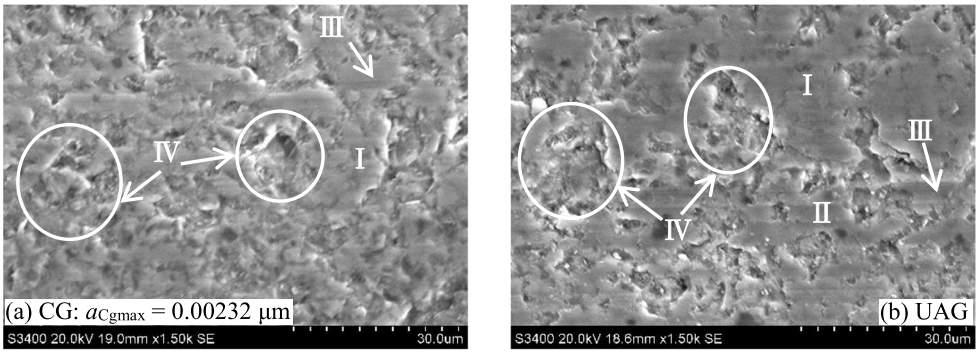

(2) v_s = 20 m/s, v_w = 0.05 m/min, a_p = 15 μm

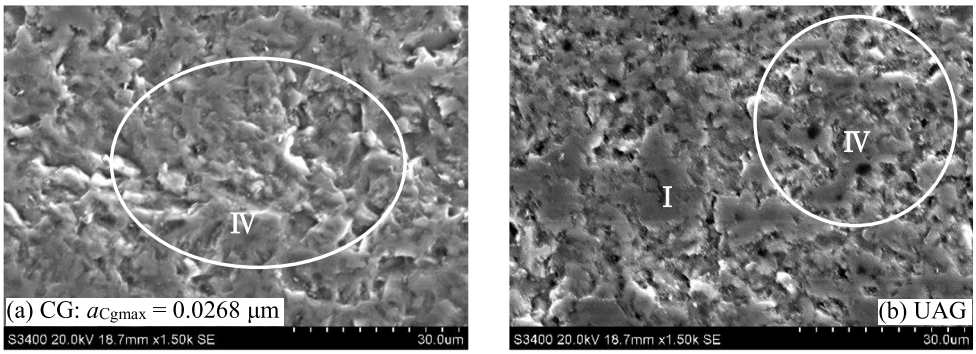

(3) v_s = 10 m/s, v_w = 0.5 m/min, a_p = 5 μm

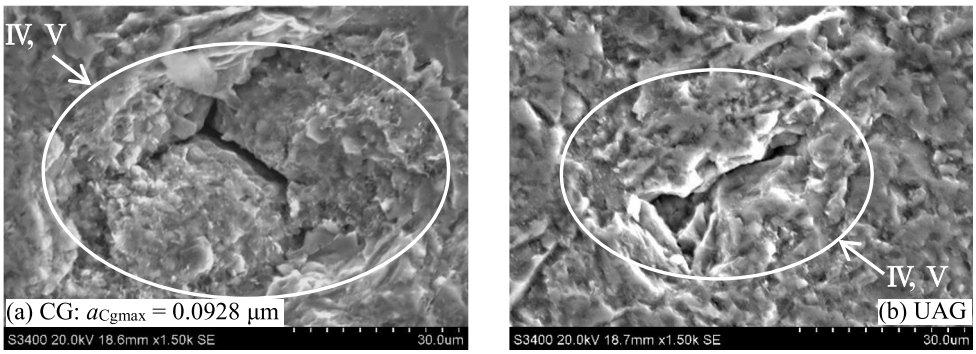

(4) v_s = 10 m/s, v_w = 1 m/min, a_p = 15 μm

(I) Smooth area; (II) porosity; (III) plastic groove; (IV) brittle fracture; (V) micro crack

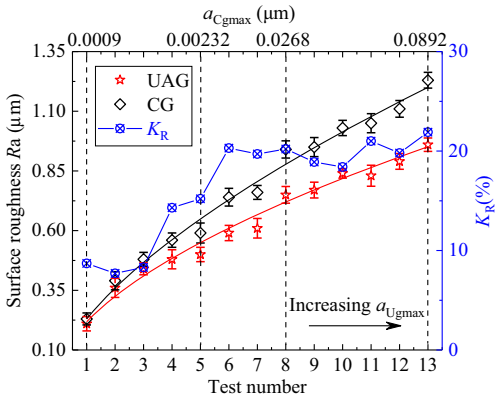

Fig. 12 Surface roughness *vs* a_{Ugmax} and a_{Cgmax}

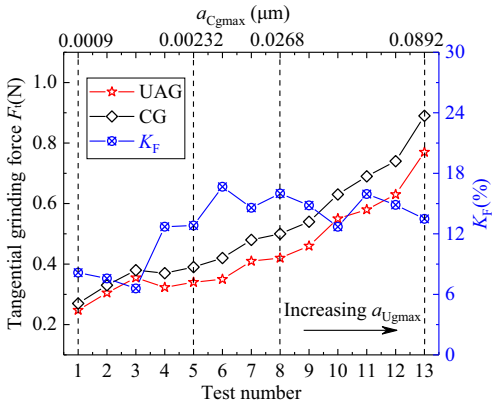

Fig. 14 Tangential grinding force *vs* a_{Ugmax} and a_{Cgmax}

subsurface breakage between UAG and CG. Under this condition, a_{Cgmax} was 0.0009 μm. Accordingly, the subsurface breakages produced by the two grinding processes were both small-sized disperse micro-fracture. In addition, b_C and b_U were both about 10 μm.

For v_s = 20 m/s, v_w = 0.05 m/min, and a_p = 10 μm, the a_{Cgmax} was 0.0019 μm. The a_{Ugmax} also increased. The corresponding subsurface micro-morphology is shown in Fig. 16 (2). Compared with Fig. 16 (1), b_C and b_U increased from 10 to 40 μm and 25 μm, respectively. The parameter $\Delta b = b_C - b_U$ is defined to evaluate the difference between UAG and CG, and it was also found that Δb increased from 0 to 15 μm. In addition, it can be seen that the dispersed micro fracture areas enlarged and followed a connectivity trend. As shown in Fig. 16 (3), b_C increased to 60 μm when a_{Cgmax} increased to 0.0268. Meanwhile, b_U increased to 45 μm with increasing of a_{Ugmax}. However, the corresponding Δb still remains 15 μm. Under this condition, the breakage areas are full of large-sized brittle fractures and exfoliation. Fig. 16 (4) shows the subsurface micro-morphology obtained in CG and UAG for v_s = 10 m/s, v_w = 1 m/min, and a_p = 15 μm. The related a_{Cgmax} was 0.0928 μm, and a_{Ugmax} further increased. Accordingly, b_C and b_U increased to 90 μm and 60 μm, respectively. Moreover, Δb significantly increased to 30 μm. In particular, large-sized cracks form under this condition.

Subsurface breakage is a common phenomenon during the grinding of ceramics, in both UAG and CG. Its formation can be attributed to the "edge fragmentation" effect [41]. In detail, the edge fragmentation effect indicates that during the machining of the workpiece, the edge areas are always subject to high stress, which results in brittle fracture and exfoliation of the material. In addition, the formation mechanism of the edge fragmentation effect is similar to that of the lateral cracks caused by grinding force according to the indentation fracture mechanics model [42]. Thus, when a_{Cgmax} and a_{Ugmax} are small, the grinding forces are also small. Accordingly, the subsurface breakages produced in CG and UAG are both dispersed micro-fracture as illustrated in Fig. 16 (1). These results correspond well to the plastic removal mechanism of the ground surface as shown in Fig. 11 (1). While grinding forces grow with increasing a_{Cgmax} and a_{Ugmax}, dispersed micro-fracture gradually expand and connect with each other. As a result, large pieces of material peel from the workpiece, and cracks are induced during CG as shown in Fig. 16 (4). Moreover, the deviations of the subsurface breakage between CG and UAG increase with increasing a_{Cgmax}, a_{Ugmax}, and K_F.

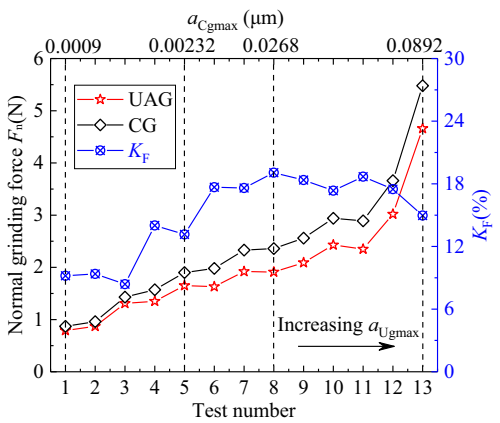

Fig. 13 Normal grinding force *vs* a_{Ugmax} and a_{Cgmax}

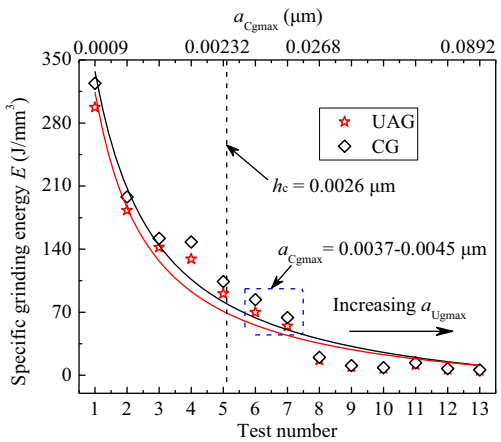

Fig. 15 Specific grinding energy *vs* a_{Cgmax} and a_{Ugmax}

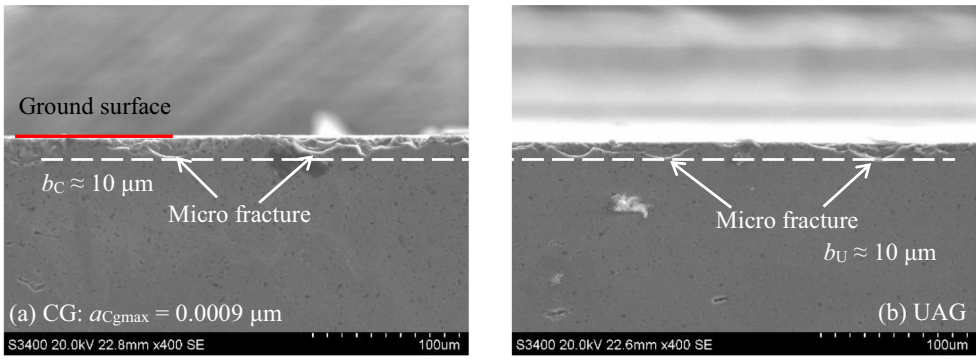

(1) $v_s = 30$ m/s, $v_w = 0.05$ m/min, $a_p = 5$ μm

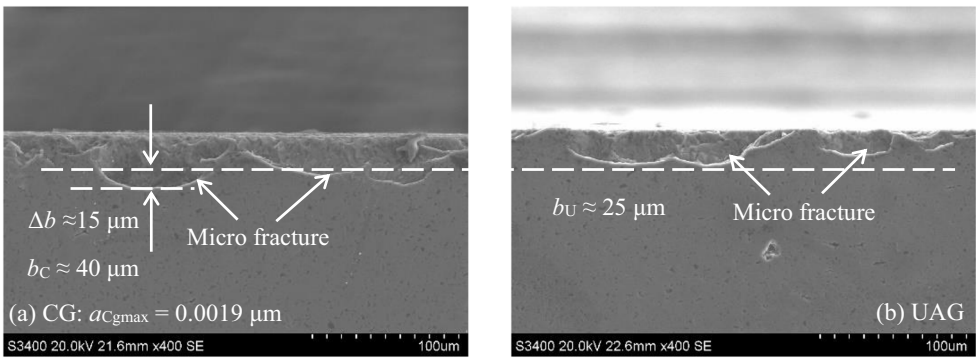

(2) $v_s = 20$ m/s, $v_w = 0.05$ m/min, $a_p = 10$ μm

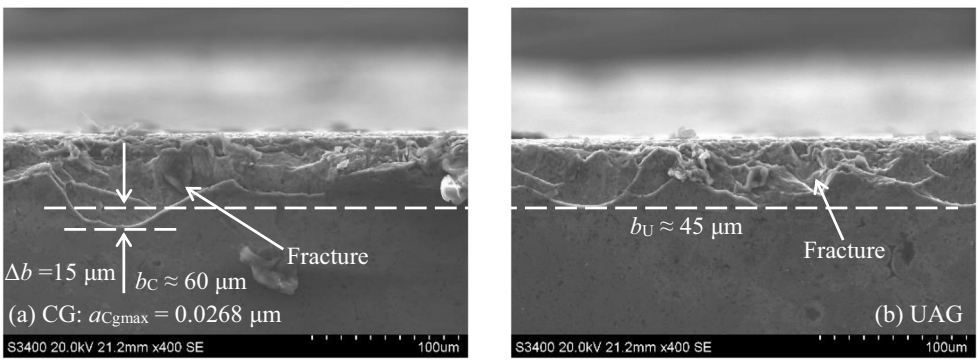

(3) $v_s = 10$ m/s, $v_w = 0.5$ m/min, $a_p = 5$ μm

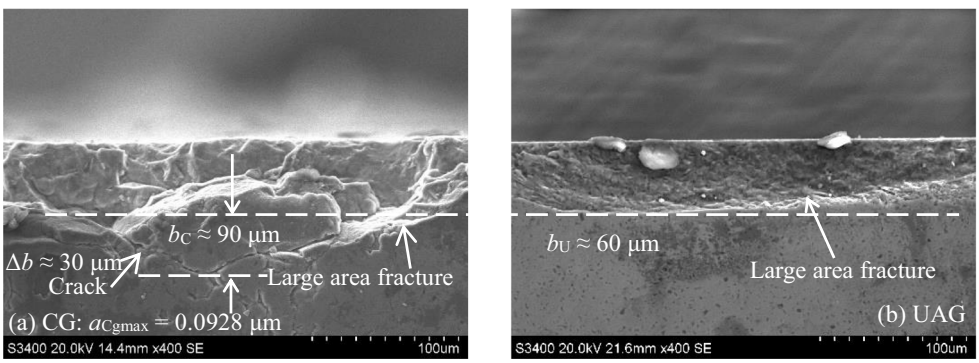

(4) $v_s = 10$ m/s, $v_w = 1$ m/min, $a_p = 15$ μm

Fig. 16 Subsurface breakage during UAG and CG of SiC. (**1**) $v_s = 30$ m/s, $v_w = 0.05$ m/min, $a_p = 5$ μm. (**2**) $v_s = 20$ m/s, $v_w = 0.05$ m/min, $a_p = 10$ μm. (**3**) $v_s = 10$ m/s, $v_w = 0.5$ m/min, $a_p = 5$ μm. (**4**) $v_s = 10$ m/s, $v_w = 1$ m/min, $a_p = 15$ μm

In summary, in UAG of SiC ceramics, based on the defined diamond grain distribution brazed grinding wheel, ultrasonic vibration is beneficial to cause ductile removal mode compared to CG, as reflected by the ground surface micro-

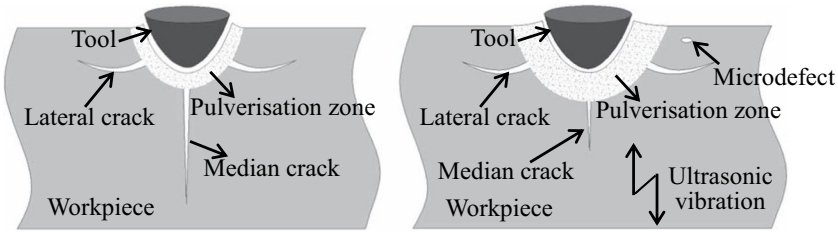

(a) Conventional machining, (b) ultrasonically-assisted machining

Fig. 17 Material damage induced in conventional and ultrasonically assisted machining [43]. **a** Conventional machining and **b** ultrasonically assisted machining

morphology, ground surface roughness, specific grinding energy, and subsurface micro-morphology. In addition, these results also indicate the feasibility to use the defined diamond grain distribution grinding wheel to control the material removal mechanism via reasonable selection of grinding parameters to acquire high machining quality during UAG of hard and brittle materials.

4.5 Discussion on ultrasonic vibration effect

The experimental results show that UAG produces less breakage compared to CG, or in other words, UAG is beneficial to obtain higher ductile removal ratio than CG on the ground surface. For the mechanism of ultrasonic vibration effect on the grinding process, there are two main academic views.

The first, it was the ductile-regime grinding theory of brittle materials proposed by Bifano [12]. According to this theory, whether the material removal mechanism during UAG is brittle fracture or ductile mode depends on size relation between the a_{Ugmax} and the critical depth of the cut. However, on the one hand, just as stated in the Section 2, there is still no widely accepted mathematical model for a_{Ugmax}. On the other hand, through single abrasive grain grinding tests, Liang [15] and Zhou [18] both showed that ultrasonic vibration could significantly increase the critical depth of cuts in hard and brittle materials. While for SiC, the ultrasonic vibration effect on this critical value is uncertain. Thus, although the research of UAG theory has made great progress, ductile-regime grinding theory in this field still needs further study.

The second, a number of researchers reported other theoretical perspectives compared with ductile regime grinding. Yang and Zhang [43] suggested that during ultrasonically assisted machining, the higher speed and acceleration led to a high strain rate, which might evoke material embrittlement in the machining process. Accordingly, the material resistance ahead of the crack tip increased with the strain-rate and impeded crack propagation as shown in Fig. 17. In addition, they also suggested that at a higher cutting speed, a median crack, if nucleated, had less time to propagate before the cutting tool passes by, which results in a smaller depth of the subsurface damage. For UAG, these theoretical perspectives are interesting and worthwhile for in-depth study.

5 Conclusions

(1) Analysis of the ground surface micro-morphology indicates that with increasing of a_{Ugmax}, the material removal mechanism in UAG of SiC changes from ductile mode to brittle fracture. This phenomenon is highly consistent with that in CG of SiC. In addition, the differences of the ground surface micro-morphology between UAG and CG under the same operating conditions gradually increase with increasing a_{Cgmax} and a_{Ugmax}.

(2) Compared with CG, UAG can produce lower ground surface roughness under similar operating conditions. In addition, K_{R} first increases slowly with increasing a_{Cgmax} and a_{Ugmax} and then stabilises. The maximum K_{R} is 22.8% under experimental conditions.

(3) Under experimental conditions, the grinding force used by UAG is always lower than that produced by CG. The change trend of K_{F} with changes in a_{Cgmax} and a_{Ugmax} shows a similar regulation with that of K_{R}. Compared with CG, UAG can decrease the K_{F} of F_{n} by 9.2–19% and the K_{F} of F_{t} by 8.1–16.7%. Based on the tangential grinding force, it can be concluded that the specific grinding energy first decreases rapidly with increasing a_{Cgmax} and a_{Ugmax} and then stabilises.

(4) For both UAG and CG, the type of subsurface breakage changes from small-sized disperse micro-fractures to large-sized brittle fracture with increasing a_{Cgmax} and a_{Ugmax}. Compared with CG, UAG causes lower subsurface breakage, especially with increasing a_{Cgmax}, a_{Ugmax}, and K_{F}.

Author contribution Kai Ding: ideas, methodology, grinding experiments, and writing—original draft
Qilin Li: grinding experiments and data curation
Changdong Zhang: resources and software

Funding This work was supported by the National Natural Science Foundation of China (Grant Nos. 51805231 and 51905234) and the Fundamental Research Funds for the Central Universities (Grant No. 30917014101).

Data availability The data sets supporting the results of this article are included within the article.

Declarations

Ethics approval Not applicable

Consent to participate Consent to participate in this study was obtained from all the authors.

Consent for publication Consent for publication was obtained from all the authors.

Competing interests The authors declare no competing interests.

References

1. Guo B, Zhao QL (2017) Ultrasonic vibration assisted grinding of hard and brittle linear micro-structured surfaces. Precis Eng 48:98–106
2. Dong GJ, Zhang LM (2019) Investigation on grinding force and machining quality during rotary ultrasonic grinding deep-small hole of fluorophlogopite ceramics. Int Adv Manuf Technol 104:2815–2825
3. Uhlmann E, Bruckhoff J (2019) Interaction of tool and workpiece in ultrasonic-assisted grinding of high performance ceramics. Procedia Manuf 33:762–769
4. Dong GJ, Lang CY, Li C, Zhang LM (2020) Formation mechanism and modelling of exit edge-chipping during ultrasonic vibration grinding of deep-small holes of microcrystalline-mica ceramics. Ceram Int 46:12458–12469
5. Dong GJ, Wang L, Li C, Yu YF (2020) Investigation on ultrasonic elliptical vibration boring of deep holes with large depth-diameter ratio for high-strength steel 18Cr2Ni4WA. Int Adv Manuf Technol 108:1527–1539
6. Uhlmann E (1998) Surface formation in creep feed grinding of advanced ceramics with and without ultrasonic assistance. Ann CIRP 47:249–252
7. Gao GF, Zhao B, Xiang DH, Kong QH (2009) Research on the surface characteristics in ultrasonic grinding nano-zirconia ceramics. J Mater Process Technol 209:32–37
8. Wang Y, Lin B, Wang SL, Cao XY (2014) Study on the system matching of ultrasonic vibration assisted grinding for hard and brittle materials processing. Int J Mach Tools Manuf 77:66–73
9. Zheng FF, Wan M, Dong ZY, Zhang WH (2018) A theoretical and experimental investigation on ultrasonic assisted grinding from the single-grain aspect. Int J Mech Sci 148:667–675
10. Xie J, Li Q, Sun JX, Li YH (2015) Study on ductile-mode mirror grinding of SiC ceramic freeform surface using an elliptical torus-shaped diamond wheel. J Mater Process Technol 222:422–433
11. Pratap A, Patra K, Dyakonov AA (2019) Experimental analysis of ductile-brittle transitions for parallel and intersecting micro-slot grinding in BK-7 glass. Ceram Int 45:11013–11026
12. Bifano TG, Dow TA, Scattergood RO (1991) Ductile-regime grinding: a new technology for machining brittle materials. J Eng Ind 113:184–189
13. Pei ZJ, Ferreira PM, Haselkorn M (1995) Plastic flow in rotary ultrasonic machining of ceramics. J Mater Process Technol 48:771–777
14. Pei ZJ, Ferreira PM (1998) Modeling of ductile-mode material removal in rotary ultrasonic machining. Int J Mach Tools Manuf 38:1399–1418
15. Liang ZQ, Wang XB, Wu YB, Xie LJ, Jiao L, Zhao WX (2013) Experimental study on brittle-ductile transition in elliptical ultrasonic assisted grinding (EUAG) of monocrystal sapphire using single diamond abrasive grain. Int J Mach Tools Manuf 71:41–51
16. Jain AK, Pandey PM (2017) Modeling of un-deformed chip thickness in RUM process and study of size effects in μ-RUM. Ultrason 77:1–16
17. Chen JB, Fang QH, Wang CC, Du JK, Liu F (2016) Theoretical study on brittle-ductile transition behavior in elliptical ultrasonic assisted grinding of hard brittle materials. Precis Eng 46:104–117
18. Zhou M, Zhao PY (2016) Prediction of critical cutting depth for ductile-brittle transition in ultrasonic vibration assisted grinding of optical glasses. Int Adv Manuf Technol 86:1–10
19. Li CL, Peng Y, Chen DL, Pan TL (2018) Theoretical investigation of vertical elliptic vibration-assisted grinding (EVAG) technology. Int Adv Manuf Technol 94:2315–2324
20. Zhao B, Chang BQ, Wang XB, Bie WB (2019) System design and experimental research on ultrasonic assisted elliptical vibration grinding of Nano-ZrO_2 ceramics. Ceram Int 45(18):24865–24877
21. Ding WF, Dai CW, Yu TY, Xu JH, Fu YC (2017) Grinding performance of textured monolayer CBN wheels: Undeformed chip thickness nonuniformity modeling and ground surface topography prediction. Int J Mach Tools Manuf 122:66–80
22. Dai CW, Ding WF, Xu JH, Xu XP, Fu DK (2017) Effects of undeformed chip thickness on grinding temperature and burn-out in high-efficiency deep grinding of Inconel718 superalloys. Int Adv Manuf Technol 89:1841–1852
23. Zhang YZ, Fang CF, Huang GQ, Xu XP (2018) Modeling and simulation of the distribution of undeformed chip thicknesses in surface grinding. Int J Mach Tools Manuf 127:14–27
24. Aurich JC, Braun O, Warnecke G, Cronjager L (2003) Development of a superabrasive grinding wheel with defined grain structure using kinematic simulation. CIRP Ann Manuf Technol 52:275–280
25. Aurich JC, Herzenstiel P, Sudermann H, Magg T (2008) High-performance dry grinding using a grinding wheel with a defined grain pattern. CIRP Ann Manuf Technol 57:357–362
26. Ding WF, Barbara L, Zhu YJ, Li Z, Fu YC, Su HH, Xu JH (2017) Review on monolayer CBN superabrasive wheels for grinding metallic materials. Chin J Aeronaut 30:109–134
27. Mukhopadhyay P, Simhan DR, Ghosh A (2017) Challenges in brazing large synthetic diamond grit by Ni-based filler alloy. J Mater Process Technol 250:390–400
28. Su HH, Dai JB, Ding WF, Zhang K, Xu W (2016) Experimental research on performance of monolayer brazed diamond wheel through a new precise dressing method-plate wheel dressing. Int Adv Manuf Technol 87:3249–3259
29. Huang GQ, Yu KF, Zhang MQ, Guo H, Xu XP (2018) Grinding characteristics of aluminium alloy 4032 with a brazed diamond wheel. Int Adv Manuf Technol 95:4573–4581
30. Ding WF, Zhu YJ, Zhang LC, Xu JH, Fu YC, Liu WD, Yang CY (2015) Stress characteristics and fracture wear of brazed CBN grains in monolater grinding wheels. Wear 332-333:800–809
31. Chattopadhyay AK, Chollet L, Hintermann HE (1991) On performance of brazed bonded monolayer diamond grinding wheel. CIRP Ann 40:347–350
32. Wu QP, Ouyang ZY, Wang Y, Yang H, Song K (2019) Precision grinding of engineering ceramic based on the electrolytic dressing of a multi-layer brazed diamond wheel. Diam Relat Mater 100:107552
33. Chen JY, Shen JY, Huang H, Xu XP (2010) Grinding characteristics in high speed grinding of engineering ceramics with brazed diamond wheels. J Mater Process Technol 210:899–906
34. Hecker RL, Liang SY, Wu XJ, Xia P, Jin DGW (2007) Grinding force and power modeling based on chip thickness analysis. Int Adv Manuf Technol 33:449–459

35. Malkin S (2008) Grinding technology-theory and applications of machining with abrasives, 2th edn. Industrial Press, New York, pp 54–59
36. Agarwal S, Rao PV (2012) Predictive modeling of undeformed chip thickness in ceramic grinding. Int J Mach Tools Manuf 56: 59–68
37. Agarwal S, Rao PV (2013) Predictive modeling of force and power based on a new analytical undeformed chip thickness model in ceramic grinding. Int J Mach Tools Manuf 65:68–78
38. Bertsche E, Ehmann K, Malukhin K (2013) An analytical model of rotary ultrasonic milling. Int Adv Manuf Technol 65:1705–1720
39. Zong WJ, Cao ZM, He CL, Sun T (2015) Critical undeformed chip thickness of brittle materials in single point diamond turning. Int Adv Manuf Technol 81:975–984
40. Huang WH, Yu DP, Zhang XQ, Zhang M, Chen DS (2018) Ductile-regime machining model for ultrasonic elliptical vibration cutting of brittle materials. J Manuf Process 36:68–76
41. Zhang B, Meng J (2003) Grinding damage in fine ceramics. Nanotechnol Precis Eng 1(1):48–56
42. Malkin S, Hwang TW (1996) Grinding mechanisms for ceramics. Ann CIRP 45(2):569–580
43. Yang XX, Zhang B (2019) Material embrittlement in high strain-rate loading. Int J Extreme Manuf 1:022003